American Mineralogist, Volume 93, pages 644–652, 2008

The high-pressure behavior of an Al- and Fe-rich natural orthopyroxene

F. Nestola,[1,2,*] T. Boffa Ballaran,[3] T. Balić-Žunić,[4] L. Secco,[1] and A. Dal Negro[1]

[1]Dipartimento di Geoscienze, Università di Padova, Via Giotto 1, I-35137 Padova, Italy
[2]CNR-IGG, Sezione di Padova, Via Giotto, I-35137, Padova, Italy
[3]Bayerisches Geoinstitut, University of Bayreuth, Universitaetstrasse 37, D-95447 Bayreuth, Germany
[4]Department of Geography and Geology, University of Copenhagen, Oester Voldgade 10, DK-1350 Copenhagen, Denmark

Abstract

A single crystal of a natural orthopyroxene with composition $^{M2}[Fe^{2+}_{0.818}Mg_{0.156}Ca_{0.010}Mn_{0.016}]^{M1}[Fe^{2+}_{0.081}Mg_{0.767}Al_{0.084}Fe^{3+}_{0.068}]^{TA}[Si]^{TB}[Si_{0.848}Al_{0.152}]O_6$ and space group *Pbca* (sample S95) was investigated at high pressure by X-ray diffraction using a diamond-anvil cell up to 9.56 GPa. No phase transitions were detected in the pressure range investigated. The unit-cell parameters, *a*, *b*, and *c*, decrease non-linearly with pressure and show an axial compression anisotropy with a ratio $\beta_a:\beta_b:\beta_c$ = 1.00:1.64:1.16. The unit-cell volume decreases non-linearly as well and with a negative variation, by about 6.3% up to 9.56 GPa. The equation of state calculated using high-accuracy volume-pressure data up to 5.5 GPa gave the following coefficients: V_0 = 846.02(4) Å^3, K_{T0} = 115.4(6) GPa, K' = 7.7(3). Among the Mg-orthopyroxenes investigated at high pressure so far S95 shows the highest bulk modulus.

Six complete intensity data were collected at 0, 0.16, 1.72, 3.95, 8.03, and 9.56 GPa. The results confirm previous conclusions regarding the compressional mechanism in orthopyroxenes. At lower pressures, compression is mostly connected to a decrease in volume of the two M-coordination octahedra, accompanied by an increased kink in the B-tetrahedral chain. At higher pressures, compression of the M sites decreases, the kink of the tetrahedral chains stops to change, and reduction in unit-cell volume is accompanied mainly by compression of tetrahedra.

This change in compressional trends results in a relatively large K' parameter and a pronounced stiffening of the structure with pressure. The presence of Al in the TB tetrahedral site influences the kink of the B tetrahedral chain, which depends on the ratio of sizes of the M2 and TB coordination polyhedra. The increased stiffness of the M polyhedra, caused by the presence of Fe, is the main reason for the high bulk modulus of S95 and its resistance to shortening of the **c** axis. This explains the limited shortening of the **c** axis in S95 and the different compressional axial anisotropy with respect to other orthopyroxenes investigated under high pressure.

Keywords: Orthopyroxene, high pressure, crystal structure, X-ray diffraction

Introduction

Several recent studies have focused on the behavior of orthopyroxene with different compositions under extreme conditions of pressure and temperature and using different experimental and computational techniques (e.g., Angel and Jackson 2002; Miyake et al. 2004; Nestola et al. 2006; Bromiley and Bromiley 2006; Cámara and Nestola 2006; Boffa Ballaran et al. 2006; Perrillat et al. 2007; Gatta et al. 2007). The large number of investigations on orthopyroxenes is likely due to the very wide range of geological environments in which orthopyroxene is involved, from magmatic to methamorphic rocks and meteorites. In particular, orthopyroxenes are significantly abundant in the upper mantle, and most mineralogical and geophysical investigations have concentrated on shedding light on the extremely complex and geodynamic processes occurring at that depth. Knowledge of the compressional and thermal behavior of orthopyroxenes is fundamental for the understanding geological environments in which this silicate plays a crucial role.

Concerning the high-pressure behavior of orthopyroxene, X-ray diffraction studies on compressional and structural behavior have been performed on pure synthetic $MgSiO_3$ (Hugh-Jones and Angel 1994; Angel and Hugh-Jones 1994; Angel and Jackson 2002), on pure synthetic orthoferrosilite $FeSiO_3$ and along the $MgSiO_3$-$FeSiO_3$ solid solution (Hugh-Jones et al. 1997, synthetic and natural samples containing very small amounts of Al and Ca). Although the data produced in these studies concerning the bulk modulus and its first pressure derivative are consistent, the same is not true for the structural data for which several doubts remain, especially concerning the behavior of the tetrahedra and the effect of Fe, Ca, and Al admixtures at high pressure (e.g., Hugh-Jones and Angel 1994; Hugh-Jones et al. 1997; Nestola et al. 2006). More recently, Nestola et al. (2006) studied a synthetic orthopyroxene with composition $Ca_{0.07}Mg_{1.93}Si_2O_6$ and found a different crystal structural evolution with pressure compared to previous studies. Although this investigation clarified the effect of Ca, the influence of Fe and Al, which are almost always present in natural samples, is not yet fully understood.

* E-mail: fabrizio.nestola@unipd.it

The aim of this work is to define the high-pressure crystal structure evolution and the compressional behavior of a natural orthopyroxene with substantial content of Fe^{2+}, Fe^{3+}, and Al. We selected a sample with the formula $^{M2}[Fe^{2+}_{0.818}Mg_{0.156}Ca_{0.010}Mn_{0.016}]$ $^{M1}[Fe^{2+}_{0.081}Mg_{0.767}Al_{0.084}Fe^{3+}_{0.068}]^{TA}[Si]^{TB}[Si_{0.848}Al_{0.152}]O_6$. This crystal is sample S95 previously studied by Tazzoli and Domeneghetti (1987) at room pressure, for which the Fe^{3+}/Fe^{2+} ratio has been determined by Mössbauer spectroscopy, and cation distribution determined by single-crystal X-ray diffraction.

Here, the orthopyroxene S95 is investigated by single-crystal X-ray diffraction using a diamond anvil cell up to about 10 GPa at room temperature. The equation of state is determined from measurement of unit-cell parameters on a high-precision Huber diffractometer equipped with a point detector, as described in Hugh-Jones and Angel (1994), Angel and Hugh-Jones (1994), Hugh-Jones et al. (1997), Angel and Jackson (2002), and Nestola et al. (2006), to provide direct comparison with these previous studies. Crystal structure at high pressure is determined from measurements on a diffractometer equipped with a CCD detector. This work is part of a wider project focused on the high-pressure behavior of natural and synthetic orthopyroxenes involving the Bayerisches Geoinstitut in Bayreuth, the Geocenter in Copenhagen and the Department of Geosciences in Padova.

Experimental methods

An inclusion- and twin-free single crystal of the S95 sample, selected from the same crystal batch of Tazzoli and Domeneghetti (1987), brown in color, perfectly transparent and with crystal size of 180 × 80 × 50 μm^3 was chosen for the high-pressure single-crystal X-ray diffraction experiment. The crystal was loaded in a BGI-type diamond anvil cell using a steel gasket T301 and a 16:3:1 mixture of methanol:ethanol:water as a pressure transmitting medium. The gasket was preindented at 90 μm in thickness and the gasket hole was 250 μm in diameter. A single crystal of quartz was used as an internal diffraction pressure standard (Angel et al. 1997). The unit-cell parameters were determined at seven different pressures up to about 5.5 GPa and room temperature on a Huber four-circle diffractometer (Mo$K\alpha$ radiation from a Mo-tube without monochromator) at Bayerisches Geoinstitut using eight-position centering of 16 Bragg reflections according to the procedure of King and Finger (1979) and Angel et al. (2000). Centering procedure and vector-least-squares refinement of the unit-cell constants were performed by SINGLE04 software according to the protocol of Ralph and Finger (1982) and Angel et al. (2000). The unit-cell data at different pressures are reported in Table 1. At 5.5 GPa, the gasket started to collapse and the crystal (not touched by the diamonds) was recovered from the DAC. After checking that the Bragg reflection width remained constant, the crystal was loaded again in the same DAC and complete intensity data were measured, this time at the Geological Institute of Copenhagen using a Bruker-AXS four-circle diffractometer equipped with a Smart1000 CCD area detector (6.25 × 6.25 cm active area with a resolution of 81.92 pixels cm^{-1}) and a flat graphite monochromator, using Mo$K\alpha$ radiation. Before loading the crystal for the second time, a complete intensity data collection with the crystal in air was done on this diffractometer with the results reported in Table 2 (the second column). It can be observed that the unit-cell volumes at ambient conditions determined at Bayerisches Geoinstitut reported in Table 1 and that measured at Geological Institute of Copenhagen (Table 2) are in perfect agreement, with differences less than one standard deviation. We therefore decided not to load any internal pressure standard in the DAC and used the equation of state determined by the pressure-volume data of Table 1 (see in the "Results" section for the calculation details) measured on the same crystal for the pressure calibration. Five complete data collections at P = 0.16, 1.72, 3.95, 8.03, and 9.56 GPa using a sample-to-detector distance of 5.5 cm were performed with the crystal in the DAC. A total of 1800 exposures (frame width = 0.2°, time = 30 s) were collected at every pressure. The data collections were made in 16 separate ω-scans covering practically all of the available reciprocal space up to 60° in 2θ. Each scan covered a span of 20° in ω with detector (2θ circle) positioned so as to be parallel to the planes of the gasket and culet faces in the middle of the scan range. This orientation of the detector relative to DAC escapes completely the blind regions (secondary X-rays shaded by the DAC body) at the applied sample-detector distance. Eight of the scans were performed with ϕ setting adjusted so that the primary beam was entering one side of the DAC, the other eight with ϕ setting 180° apart, and primary beam entering the other side of DAC first, in this way ensuring best conditions for the refinement of the crystal displacement from the goniometer center. In each group of runs, four were performed with χ set to 0°, which makes ϕ and ω axes coincident, summing to a total sweep angle for the primary beam of 80° from both sides of the DAC, covering close to a full opening angle of the beryllium window. The remaining scans were performed with χ set to various angles ensuring the best coverage of the rest of the unshaded reciprocal space. The data collection strategy, with differences in ω and 2θ angles less than 15° minimized the potential shadowing effect of the gasket on the crystal. SMART software was used for lattice determination and data collection. Data were integrated with SAINT+ and corrected for absorption using SADABS software (Bruker 2000) leading to a significant improvement in R_{int}. The SADABS correction was applied for the complex absorption effects, where an empirical function based on measurements of symmetry equivalents (over 440 reflections with $I > 4\sigma$) and modeled upon spherical harmonics (with three odd and six even orders) was used. SADABS also removes the "outlier" reflections with $|I - \langle I\rangle| / [\sigma 2 + (0.04 \langle I\rangle)^2] > 4$.

Weighted structural refinements were done using the SHELX-97 package (Sheldrick 1997). As no violation in symmetry was detected with increasing pressure, all refinements were performed in *Pbca* space group starting from the atomic coordinates of Nestola et al. (2006) and using the cation distribution published for S95 by Tazzoli and Domeneghetti (1987). The refinements were done using neutral scattering factors for all the atoms. For the room-pressure data this refinement procedure gave the same bond distances as published by Tazzoli and Domeneghetti (1987) for the sample S95. The M2 and M1 sites were refined with anisotropic displacement parameters at ambient conditions and at all pressures, whereas the other sites were refined anisotropically only at ambient conditions. Crystal and refinement data together with the unit-cell parameters are reported in Table 2, atomic coordinates and displacement parameters in Table 3, while the bond distances, polyhedral volumes, tetrahedral chain kinking angles, quadratic elongation and angle variance (Robinson et al. 1971), and polyhedral distortion parameters (Balić-Žunić 2007) are reported in Table 4. For all structures the volumes and their standard deviations are calculated by IVTON (Balić-Žunić and Vickovic 1996).

Table 1. Unit-cell parameters at different pressures for the S95 orthopyroxene investigated in this study (data measured on point detector at Bayreuth)

P (GPa)	a (Å)	b (Å)	c (Å)	V (Å^3)
*0.00010(1)	18.2920(3)	8.8637(4)	5.2179(3)	845.99(6)
1.183(4)	18.2450(3)	8.8258(5)	5.2025(3)	837.75(6)
1.796(4)	18.2220(3)	8.8063(4)	5.1951(3)	833.65(6)
2.551(6)	18.1944(2)	8.7838(4)	5.1862(3)	828.84(6)
3.166(6)	18.1726(3)	8.7667(4)	5.1796(2)	825.19(5)
4.521(6)	18.1292(4)	8.7293(7)	5.1659(4)	817.53(9)
5.548(7)	18.0973(5)	8.7015(8)	5.1558(5)	811.91(11)

* With crystal in the DAC.

Results

Compressibility

The evolution of the unit-cell parameters and cell volume with pressure are reported in Figures 1a and 1b. A continuous decrease of the unit-cell constants and volume is observed as a function of pressure with no evidence of a phase transition up to the maximum pressure reached. This was also confirmed by the crystal-structure data collected up to about 9.5 GPa. From Figure 1a, it is evident that the b direction undergoes the maximum compression, whereas a is the least compressible direction. The unit-cell volume decreases by about 4% up to 5.5 GPa. The volume-pressure data were fitted using a third-order Birch-Murnaghan equation of state (BM3; Birch 1947) using EoS-FIT5.2 software (Angel 2002). Refining simultaneously the volume, V_0, the bulk modulus K_{T0}, and its first pressure derivative K' we obtained the following coefficients: V_0 = 846.02(4) Å^3, K_{T0} =

TABLE 2. Crystal data and refinement results at different pressures for the S95 orthopyroxene studied in this work (data collected on a CCD at Copenhagen)

P (GPa)	0*	0†	0.163	1.715	3.947	8.033	9.562
a (Å)	18.2889(11)	18.2889(11)	18.2804(5)	18.2192(5)	18.1427(5)	18.0221(5)	17.9770(5)
b (Å)	8.8662(5)	8.8662(5)	8.8601(3)	8.8111(5)	8.7460(3)	8.6456(3)	8.6100(3)
c (Å)	5.2175(3)	5.2175(3)	5.2161(3)	5.1965(3)	5.1716(3)	5.1327(3)	5.1227(3)
V (Å^3)	846.03(3)	846.03(3)	844.84(6)	834.20(5)	820.61(5)	799.73(5)	792.90(5)
Space group	*Pbca*	*Pbca*	*Pbca*	*Pbca*	*Pbca*	*Pbca*	*Pbca*
Unique reflections	1289	669	741	719	702	690	682
Reflections >4σ	925	458	499	482	464	457	443
$R_{4\sigma}$ (%)	2.54	2.95	5.76	5.37	5.05	5.19	5.49
$2\theta_{max}$ (°)	61.04	60.90	58.06	57.45	58.30	57.91	58.08
R_{all} (%)	4.22	4.70	9.88	9.62	9.28	9.31	9.87
R_{int} (%)	5.43	4.28	6.55	6.84	6.46	6.87	7.34
GooF	0.81	0.84	1.05	1.06	0.94	0.95	0.98
Parameters	92	52	52	52	52	52	52

Notes: All the data were refined using SHELXL-97 (Sheldrick 1997). The reflections were calculated using the DAC_RESTRICT software (Angel, unpublished), which is capable of calculating not accessible reflections due to orientation of the crystal in the DAC.
* Refinement with crystal in air.
† Refinement with crystal in air but performed using the same number of reflections with respect to that accessible with the crystal in the DAC.

TABLE 3. Atomic coordinates and thermal parameters *U* (Å^2) at different pressures for the S95 orthopyroxene investigated in the present work

P (GPa)		0*	0†	0.163	1.710	3.947	8.033	9.562
M2	*x*	0.37965(2)	0.37962(3)	0.37962(5)	0.37964(5)	0.37963(5)	0.37954(5)	0.37946(6)
	y	0.48140(4)	0.48150(9)	0.4811(1)	0.4803(1)	0.4792(1)	0.4777(1)	0.4772(1)
	z	0.36168(6)	0.3618(1)	0.3614(3)	0.3588(3)	0.3568(3)	0.3544(4)	0.3536(4)
	U_{eq}	0.0084(1)	0.0086(2)	0.0110(5)	0.0109(5)	0.0100(5)	0.0089(6)	0.0085(6)
M1	*x*	0.37580(4)	0.37582(5)	0.37577(9)	0.37578(9)	0.37582(9)	0.37601(9)	0.3762(1)
	y	0.65423(7)	0.65443(2)	0.6542(2)	0.6552(2)	0.6559(2)	0.6572(2)	0.6579(2)
	z	0.8690(1)	0.86913(2)	0.8687(6)	0.8664(6)	0.8644(5)	0.8612(6)	0.8598(6)
	U_{eq}	0.0074(1)	0.0066(4)	0.0110(7)	0.0103(8)	0.0099(8)	0.0094(8)	0.0095(8)
TA	*x*	0.27129(3)	0.27142(5)	0.27140(9)	0.27127(9)	0.27112(8)	0.27097(9)	0.2709(1)
	y	0.34091(7)	0.3411(2)	0.3406(2)	0.3410(2)	0.3418(2)	0.3430(2)	0.3431(2)
	z	0.0482(1)	0.0480(2)	0.0479(6)	0.0448(6)	0.0403(6)	0.0350(6)	0.0337(6)
	$U_{eq}/_{iso}$‡	0.0056(1)	0.00564(2)	0.0058(5)	0.0064(5)	0.0061(5)	0.0056(5)	0.0058(5)
TB	*x*	0.47336(3)	0.47330(5)	0.47332(9)	0.47318(9)	0.47292(9)	0.47284(9)	0.4728(1)
	y	0.33616(7)	0.3366(2)	0.3361(2)	0.3365(2)	0.3367(2)	0.3374(2)	0.3375(2)
	z	0.8012(1)	0.8012(2)	0.8030(6)	0.8037(6)	0.8048(6)	0.8057(6)	0.8059(6)
	$U_{eq}/_{iso}$	0.0060(1)	0.0059(2)	0.0068(5)	0.0066(5)	0.0064(5)	0.0063(5)	0.0064(5)
O1A	*x*	0.18322(8)	0.1832(1)	0.1830(2)	0.1832(2)	0.1825(2)	0.1821(2)	0.1819(3)
	y	0.3375(2)	0.3382(4)	0.3370(5)	0.3370(5)	0.3373(4)	0.3376(5)	0.3376(5)
	z	0.0412(3)	0.0405(5)	0.0401(14)	0.0370(15)	0.0338(14)	0.0286(14)	0.0312(14)
	$U_{eq}/_{iso}$	0.0081(3)	0.0079(6)	0.0086(11)	0.009(1)	0.009(1)	0.008(1)	0.006(1)
O2A	*x*	0.31104(8)	0.3111(1)	0.3112(2)	0.3107(2)	0.3099(2)	0.3090(2)	0.3088(3)
	y	0.5017(2)	0.5014(4)	0.5012(5)	0.5028(5)	0.5053(5)	0.5085(5)	0.5093(5)
	z	0.0506(3)	0.0514(5)	0.0502(14)	0.0452(15)	0.0423(14)	0.0390(15)	0.0368(15)
	$U_{eq}/_{iso}$	0.0092(3)	0.0097(6)	0.0096(12)	0.010(1)	0.011(1)	0.010(1)	0.010(1)
O3A	*x*	0.30213(9)	0.3021(1)	0.3021(2)	0.3026(2)	0.3027(2)	0.3037(2)	0.3037(3)
	y	0.2314(2)	0.2317(4)	0.2326(5)	0.2325(5)	0.2330(5)	0.2328(5)	0.2336(5)
	z	–0.1800(3)	–0.1798(5)	–0.181(1)	–0.185(1)	–0.188(1)	–0.195(1)	–0.197(2)
	$U_{eq}/_{iso}$	0.0090(3)	0.0090(6)	0.0086(11)	0.009(1)	0.008(1)	0.008(1)	0.009(1)
O1B	*x*	0.56311(9)	0.5631(1)	0.5626(2)	0.5624(2)	0.5625(2)	0.5625(2)	0.5627(3)
	y	0.3355(2)	0.3350(4)	0.3351(5)	0.3352(5)	0.3351(4)	0.3355(5)	0.3352(5)
	z	0.8031(3)	0.8033(5)	0.8044(14)	0.8072(14)	0.8069(14)	0.8118(14)	0.8118(15)
	$U_{eq}/_{iso}$	0.0082(3)	0.0087(6)	0.0096(11)	0.008(1)	0.008(1)	0.009(1)	0.008(1)
O2B	*x*	0.43341(9)	0.4335(1)	0.4335(2)	0.4337(2)	0.4340(2)	0.4344(2)	0.4347(3)
	y	0.4855(2)	0.4851(4)	0.4857(5)	0.4868(5)	0.4879(4)	0.4897(5)	0.4898(5)
	z	0.6953(3)	0.6953(5)	0.6913(13)	0.6926(14)	0.6916(14)	0.6886(14)	0.6876(15)
	$U_{eq}/_{iso}$	0.0096(3)	0.0088(6)	0.0108(12)	0.012(1)	0.011(1)	0.011(1)	0.011(1)
O3B	*x*	0.44655(9)	0.4466(1)	0.4464(2)	0.4460(2)	0.4453(2)	0.4447(2)	0.4447(2)
	y	0.3027(2)	0.3026(4)	0.3030(5)	0.3043(5)	0.3058(5)	0.3066(5)	0.3072(5)
	z	0.1038(3)	0.1044(5)	0.1008(13)	0.1032(14)	0.1077(13)	0.1090(14)	0.1107(14)
	$U_{eq}/_{iso}$	0.0101(3)	0.0114(7)	0.0094(12)	0.010(1)	0.009(1)	0.009(1)	0.008(1)

* See Table 2.
† See Table 2.
‡ The U_{eq} were determined just for the crystal in air and for M2 and M1 at all the pressures, for the other atoms just the U_{iso} were determined at high pressure.

TABLE 4. Selected bond distances, polyhedral volumes, angles and polyhedral distortion parameters for the S95 crystal studied in this work

P (GPa)	0*	0†	0.163	1.715	3.947	8.033	9.562
M2-O1A (Å)	2.186(2)	2.178(3)	2.186(5)	2.181(5)	2.164(5)	2.141(5)	2.142(5)
M2-O1B (Å)	2.115(2)	2.119(3)	2.125(5)	2.122(5)	2.112(4)	2.104(5)	2.100(5)
M2-O2A (Å)	2.059(2)	2.055(2)	2.057(6)	2.067(7)	2.074(6)	2.075(7)	2.079(7)
M2-O2B (Å)	2.000(2)	2.000(3)	1.983(7)	1.995(7)	1.994(7)	1.982(7)	1.981(7)
M2-O3A (Å)	2.370(2)	2.372(3)	2.376(4)	2.353(5)	2.333(4)	2.290(4)	2.284(5)
M2-O3B (Å)	2.412(2)	2.412(3)	2.415(5)	2.372(6)	2.319(5)	2.270(5)	2.251(5)
<M2-O> (Å)	2.190	2.189	2.190	2.182	2.166	2.144	2.140
V (Å^3)‡	12.929(6)	12.921(10)	12.901(17)	12.767(22)	12.487(20)	12.068(20)	11.992(22)
volume distortion‡	0.0805	0.0801	0.0805	0.0798	0.0799	0.0813	0.0812
asphericity‡	0.1635	0.1636	0.1715	0.1521	0.1326	0.1136	0.1085
eccentricity‡	0.2135	0.2155	0.2135	0.1921	0.1774	0.1581	0.1522
M1-O1A (Å)	2.024(2)	2.027(3)	2.024(7)	2.022(7)	2.011(7)	2.003(7)	1.981(7)
M1-O1A (Å)	2.148(2)	2.148(3)	2.139(5)	2.122(5)	2.098(5)	2.066(5)	2.063(6)
M1-O1B (Å)	2.045(2)	2.044(3)	2.046(7)	2.038(7)	2.036(7)	2.012(7)	2.010(7)
M1-O1B (Å)	2.154(2)	2.150(3)	2.158(5)	2.144(5)	2.120(5)	2.096(5)	2.076(6)
M1-O2A (Å)	2.032(2)	2.036(3)	2.032(6)	2.018(6)	2.003(5)	1.986(6)	1.982(6)
M1-O2B (Å)	2.042(2)	2.047(3)	2.050(6)	2.033(6)	2.018(5)	1.998(5)	1.995(6)
<M1-O> (Å)	2.074	2.075	2.075	2.063	2.048	2.027	2.018
V (Å^3)‡	11.759(6)	11.783(9)	11.771(16)	11.589(19)	11.338(17)	10.997(17)	10.852(19)
volume distortion‡	0.0097	0.0097	0.0096	0.0082	0.0081	0.0078	0.0080
asphericity‡	0.0412	0.0453	0.0449	0.0376	0.0271	0.0223	0.0253
eccentricity‡	0.1090	0.1043	0.1063	0.1072	0.1006	0.0925	0.0858
TA-O1A (Å)	1.611(2)	1.615(2)	1.616(5)	1.606(5)	1.610(4)	1.602(4)	1.601(6)
TA-O2A (Å)	1.600(2)	1.596(4)	1.599(5)	1.596(5)	1.593(4)	1.587(4)	1.585(5)
TA-O3A (Å)	1.636(2)	1.634(3)	1.630(6)	1.634(6)	1.619(6)	1.626(7)	1.623(8)
TA-O3A (Å)	1.656(2)	1.658(3)	1.653(7)	1.648(7)	1.655(7)	1.645(7)	1.639(9)
<TA-O> (Å)	1.626	1.626	1.624	1.621	1.619	1.615	1.612
V (Å^3)‡	2.179(2)	2.176(4)	2.174(6)	2.161(8)	2.153(7)	2.135(7)	2.125(10)
volume distortion‡	0.0097	0.0096	0.0097	0.0088	0.0084	0.0093	0.0085
eccentricity‡	0.0708	0.0759	0.0672	0.0683	0.0722	0.0709	0.0680
TB-O1B (Å)	1.641(2)	1.642(2)	1.631(5)	1.625(5)	1.625(4)	1.616(4)	1.616(6)
TB-O2B (Å)	1.610(2)	1.602(3)	1.620(5)	1.614(5)	1.610(5)	1.605(5)	1.599(6)
TB-O3B (Å)	1.678(2)	1.678(4)	1.656(7)	1.658(7)	1.667(7)	1.659(8)	1.676(6)
TB-O3B (Å)	1.680(2)	1.683(3)	1.694(6)	1.694(6)	1.686(6)	1.681(6)	1.662(8)
<TB-O> (Å)	1.652	1.651	1.650	1.648	1.647	1.640	1.638
V (Å^3)‡	2.299(2)	2.294(4)	2.292(7)	2.280(8)	2.278(7)	2.251(8)	2.242(8)
volume distortion‡	0.0059	0.0063	0.0064	0.0059	0.0050	0.0049	0.0049
eccentricity‡	0.0922	0.1022	0.0918	0.1004	0.0996	0.1003	0.1016
(O3-O3-O3)A°	194.18(7)	194.41(14)	193.48(13)	193.51(15)	193.12(15)	193.22(14)	192.58(16)
(O3-O3-O3)B°	140.65(6)	140.58(12)	140.39(14)	139.54(12)	138.64(16)	138.25(12)	137.95(15)

* See Table 2.
† See Table 2.
‡ Calculated using program IVTON (Balić-Žunić and Vickovic 1996).

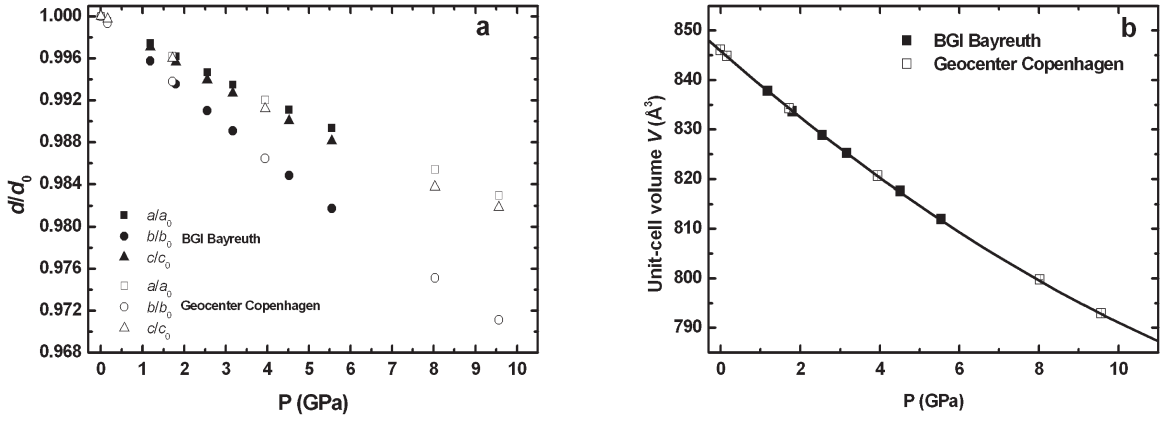

FIGURE 1. Evolution of the unit-cell parameters (**a**) and unit-cell volume (**b**) with pressure for the sample S95 studied in this work.

115.4(6) GPa, K' = 7.7(3). The F_E-f_E plot (see Angel 2001 for more details) reported in Figure 2 provides EoS coefficients with values within one standard deviation of those obtained by the direct refinement: K_{T0} = 115.9(5) GPa and K' = 7.5(2) (from F_E-f_E plot).

A parameterized form of the BM3 was used to determine the axial moduli of *a*, *b*, and *c* again using EoS-FIT5.2. All the equation-of-state coefficients together with the relative axial

compressibilities, calculated using the relation for unit-cell parameters $\beta = -1/3K_{T0}$, are reported in Table 5. The compressibility ratio using the data reported in Table 5 is $\beta_a:\beta_b:\beta_c = 1.00:1.64:1.16$ whereas the direct linear axial compressibility (for purpose of comparison with other samples calculated as $[(d - d_0)/d_0]/\Delta P$ where d and d_0 are unit-cell constants at P and P_0, respectively) gives as a ratio 1.00:1.72:1.11 again confirming that the b axis is the most compressible direction. The compressibility scheme $\beta_b > \beta_c \geq \beta_a$ is similar to that of other orthopyroxenes, but S95 shows, in this respect, a significantly smaller anisotropy.

Crystal-structure evolution with pressure

The evolution of the volumes and distortion parameters of M and T coordination polyhedra with pressure are shown in Figures 3 to 6. One can see that the data obtained in this work and by Nestola et al. (2006) show significantly smaller variation than older data on the pure enstatite and en_{60} (e.g., Hugh-Jones et al. 1997). This is expected due to the higher instrumental precision currently available, testifying to more reliable measurements of intensities of reflections. Due to a high scatter of the data for the two latter samples, it is difficult to compare details in the behavior of different coordination polyhedra among all of the samples, but the relations between general trends can be discerned. Note that the fifth enstatite so far investigated under the high pressure, the natural sample of the composition $(Mg_{0.83}Fe_{0.12}Ca_{0.006}Al_{0.04})(Si_{0.97}Al_{0.03})O_3$ (Hugh-Jones et al. 1997), is excluded from figures for better clarity, because its data mostly overlap with those of S95 and en_{60}, and show large non-systematic deviations.

The distortion parameters used in this work are the eccentricity (describing the displacement of the central atom in a coordination polyhedron from the ideal center of the polyhedron), asphericity (describing the deviation of the atoms bonded to the central atom from the surface of a circumscribed sphere), and the volume distortion (describing the volume deficit of the polyhedron as compared to an ideal one inscribed in a sphere of the same radius) (Balić-Žunić and Makovicky 1996; Balić-Žunić 2007). The advantage of these parameters is that they discriminate between distortions due to the arrangement of atoms forming the vertices of the polyhedron alone, and ones due to the relative position of the central atom and surrounding atoms. As a result, the asphericity and volume distortion can also be calculated for structural voids. Note that the asphericity for polyhedra with CN4 is zero by definition, because a common sphere can always be defined for the four points in the space. However, to our knowledge no formalism to calculate the estimated standard deviations of distortion parameters exists at the moment. Therefore, we made some calculations applying random deviations of atomic parameters according to their estimated standard deviations. A check of the induced changes to the distortion parameters suggests that the estimated standard deviations of volume distortions and asphericities are lower than 0.002, whereas the eccentricities are lower than 0.006. This applies for the present structure determinations and Ca-containing enstatite (Nestola et al. 2006), whereas for the pure enstatite and en_{60} (Hugh-Jones and Angel 1994; Hugh-Jones et al. 1997) with substantially higher e.s.d. values of atomic parameters, accordingly higher e.s.d. values of distortion parameters can be expected.

TABLE 5. EoS coefficients for the S95 sample studied in this work

a_0 (Å)	18.2921(3)
K_{a0} (GPa)	146(1)
K'	10.7(6)
β_{a0} (GPa^{-1})	–0.00228(2)
b_0 (Å)	8.8637(4)
K_{b0} (GPa)	89(1)
K'	4.4(5)
β_{b0} (GPa^{-1})	–0.00375(4)
c_0 (Å)	5.2179(3)
K_{c0} (GPa)	126(3)
K'	12(1)
β_{c0} (GPa^{-1})	–0.00264(7)
V_0 (Å^3)	846.02(4)
K_{T0} (GPa)	115.4(6)
K'	7.7(3)
β_{V0} (GPa^{-1})	–0.00866(5)

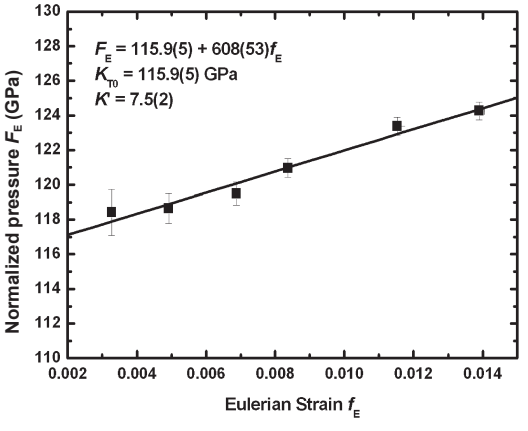

FIGURE 2. F_E-f_E plot for the S95 sample investigated in this work. In the plot the relation between F_E and f_E is reported together with the bulk modulus K_{T0} and its first pressure derivative K' obtained by the relation (for more detail see Angel 2001).

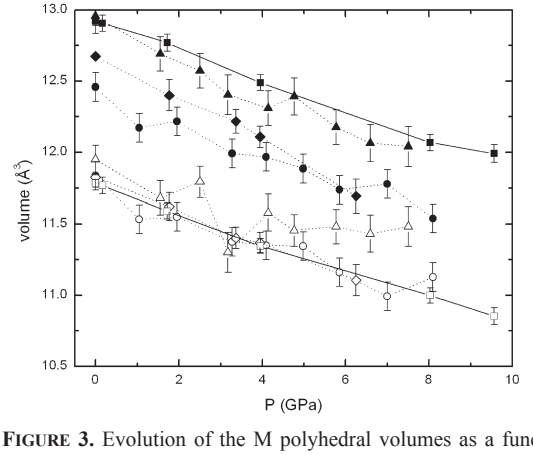

FIGURE 3. Evolution of the M polyhedral volumes as a function of pressure. The filled symbols represent M2, the empty M1. Squares = S95 (this work); circles = pure enstatite (Hugh-Jones and Angel 1994); triangles = synthetic en_{60} (Hugh-Jones et al. 1997); rhombs = Ca-containing enstatite (Nestola et al. 2006).

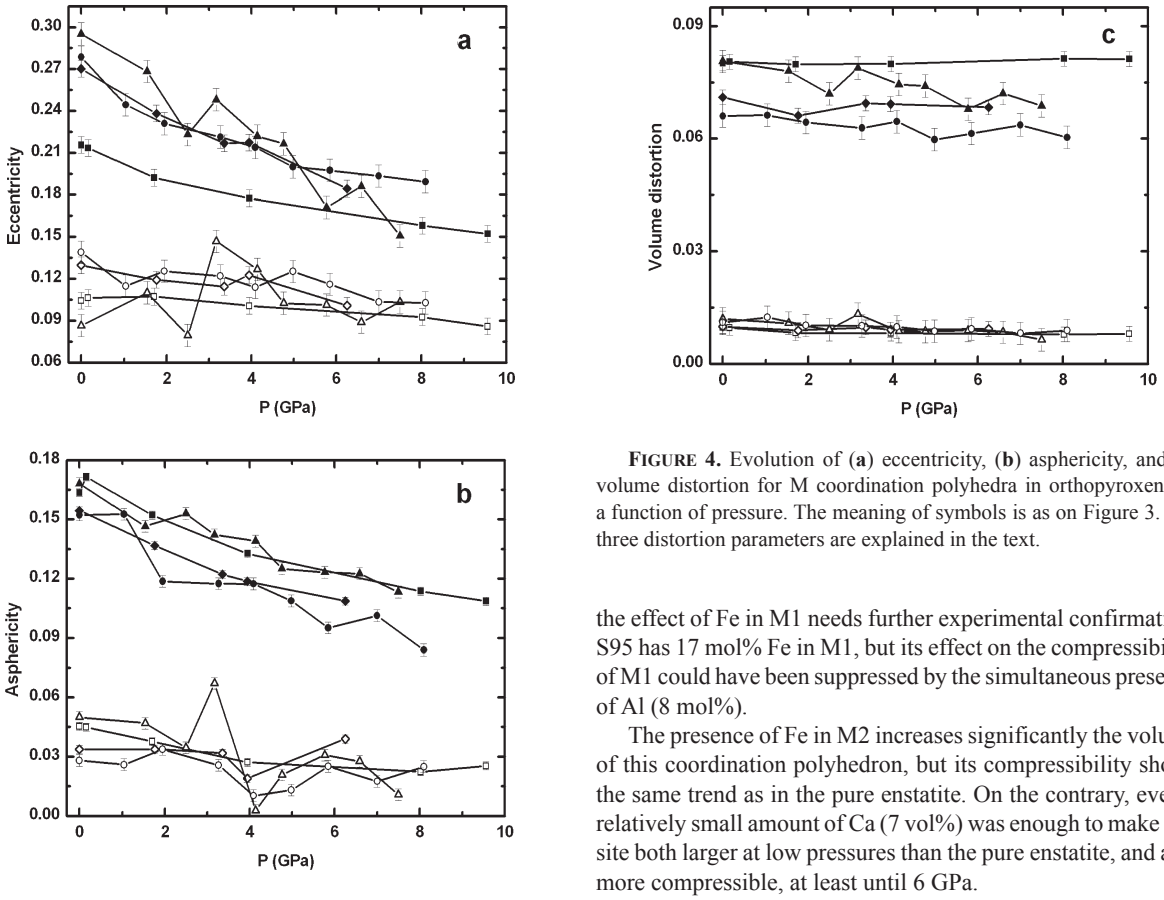

FIGURE 4. Evolution of (**a**) eccentricity, (**b**) asphericity, and (**c**) volume distortion for M coordination polyhedra in orthopyroxene as a function of pressure. The meaning of symbols is as on Figure 3. The three distortion parameters are explained in the text.

M2 and M1 octahedra

The evolution of the volumes of M octahedra with pressure is shown in Figure 3. Volumes as well as distortion parameters decrease non-linearly as a function of pressure. Comparing the compressibilities of the M coordinations in orthopyroxene the following conclusions can be made. M1 coordinations show very similar values of both volumes and their compressibilities in all investigated samples except the synthetic orthopyroxene en_{60} (Hugh-Jones et al. 1997), which shows the largest volume and has a smaller compressibility than other samples. The volumes of M2 in S95 and orthopyroxene en_{60} are similar and significantly larger than in the pure enstatite (Hugh-Jones and Angel 1994) and show similar evolution with pressure. M2 in Ca-enstatite (Nestola et al. 2006) has, at room conditions, a volume that is between those of Fe-containing samples and the pure enstatite, but shows also the largest compressibility and its volume becomes similar to that of the latter at pressures over 5 GPa.

Considering the content in the two M sites, it appears that the presence of Fe in M1 makes this site less compressible. Synthetic en_{60} orthopyroxene is reported to have equal amounts (41 mol%) of Fe in both octahedral sites (Hugh-Jones et al. 1997; atomic parameters obtained through AMS crystal structure database) that is somewhat unusual considering the preference of Fe for the M2 site. The volume of this site in en_{60} is very similar to that of S95, which has 82 mol% Fe in M2. Considering this ambiguity, the effect of Fe in M1 needs further experimental confirmation. S95 has 17 mol% Fe in M1, but its effect on the compressibility of M1 could have been suppressed by the simultaneous presence of Al (8 mol%).

The presence of Fe in M2 increases significantly the volume of this coordination polyhedron, but its compressibility shows the same trend as in the pure enstatite. On the contrary, even a relatively small amount of Ca (7 vol%) was enough to make this site both larger at low pressures than the pure enstatite, and also more compressible, at least until 6 GPa.

Distortion parameters of M polyhedra generally decrease with pressure, as expected for stable crystal structures (Balić-Žunić 2007). This decrease is larger for the M2 polyhedron, which is also significantly more distorted. The least influenced by pressure is the volume distortion, which also represents the smallest part of the global distortion. M2 in S95 shows a smaller eccentricity than the pure enstatite and the Ca-containing enstatite, which is in accordance with a significantly larger volume of M2 in S95. The asphericity of this site in S95 is, at the same time, larger than in the other two, which can be related to the influence of other bonds in the structure, which becomes more important in a larger, Fe-dominated site. An analysis of the M2-O bond distances provides an explanation for this. In S95, M2-O3B and M2-O3A undergo the greatest shortening by 6.18 and 3.63%, respectively (Table 4). With the exception of the M2-O1A distance, which undergoes a shortening of 1.86%, the other M2-O bond distances show contraction of less than 1%. Thus, the compressibility of M2 site is mainly driven by M2-O3B, with a smaller but significant contribution by M2-O3A. It is important to note that O3A and O3B are the O atoms, which bridge the Si atoms in the tetrahedral chains.

In contrast to M2, which shows a strong compressional anisotropy of bonds, the M1-O distances all undergo a similar shortening by between 2 and 4%. $M1\text{-}O1A_{(long)}$ and $M1\text{-}O1B_{(long)}$ exhibit the strongest shortening, by 3.96 and 3.62%, respectively (Table 4). As they are the longest bonds at ambient conditions among the M1-O bonds, such a behavior would be expected.

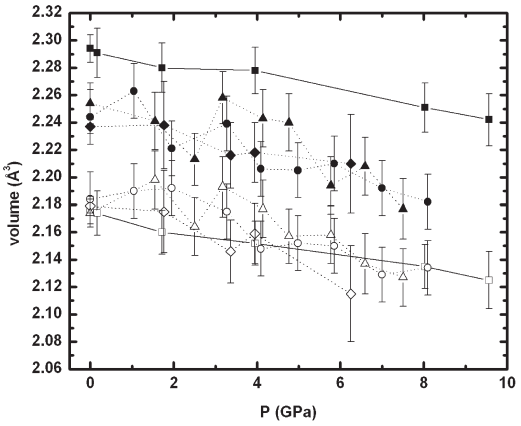

FIGURE 5. Evolution of the TA (empty symbols) and TB (full symbols) tetrahedral volumes as a function of pressure. The symbols for various orthopyroxenes correspond to those on Figure 3.

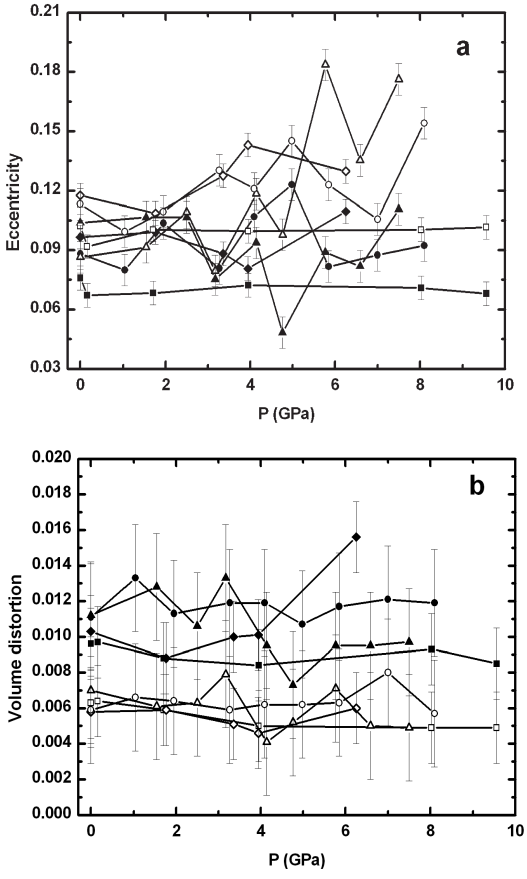

FIGURE 6. Evolution of (**a**) eccentricity and (**b**) volume distortion for T coordination polyhedra in orthopyroxene as a function of pressure. The meaning of symbols is as on Figure 3. The two distortion parameters are explained in the text.

TA and TB tetrahedra

TA and TB tetrahedra show an almost linear decrease in volume with pressure. The rate of compression is significantly lower for tetrahedral coordinations compared with the octahedral ones (in S95 their volume decrease is about 2% up to 9 GPa compared to over 7% of the octahedra).

The larger tetrahedral site (TB) has a larger eccentricity and smaller volume distortion, but the latter is generally very low for both sites. It is well known that Al-containing orthopyroxenes, Al enters the TB site (Tazzoli and Domeneghetti 1987). S95 sample has the highest Al content at TB sites among orthopyroxenes studied at high pressure so far and has, consequently, a significantly larger TB site volume. It is difficult to determine the influence of this substitution from comparison with other previously investigated enstatites due to the large scatter of data in other structure determinations. It appears that the presence of Al in TB makes this site slightly less compressible and more regular (Figs. 5 and 6).

There are no substantial differences in the compressional behavior of the two T sites. As regards the tetrahedral volumes, the TA and TB sites show similar compressibilities with a negative variation in volumes by 2.34 and 2.27%, respectively, up to 9.5 GPa (Fig. 5 and Table 4). However, the kink of the tetrahedral chains, as defined by the O3-O3-O3 angle, shows a more pronounced difference. The O3A-O3A-O3A angle (describing the kink of the A tetrahedral chain) decreases with pressure by only 0.82% whereas the smaller O3B-O3B-O3B angle from the B chain decreases by almost 2% (1.92%). As discussed later, the kink of the chain reflects a combined influence of the M2 site and the tetrahedral sites.

DISCUSSION

Among the five Mg-orthopyroxenes most recently studied at high pressure by single-crystal X-ray diffraction (Hugh-Jones and Angel 1994; Hugh-Jones et al. 1997; Angel and Jackson 2002; Nestola et al. 2006) S95 is the sample showing the highest bulk modulus K_{T0}. It also shows a different K' with respect to the other cited orthopyroxenes. Its value (K' = 7.7) is intermediate between those of orthoenstatite (Angel and Jackson 2002) and Ca-opx (Nestola et al. 2006), which show values of 8.5 and 6.6, respectively.

The higher stiffness of the S95 sample can be explained by considering its crystal structure evolution with pressure. If we compare S95 with the most recent work by X-ray diffraction on Ca-opx at high pressure (Nestola et al. 2006), we can observe some important differences: in Ca-opx, M2 volume is much more compressible than M1 and the TA volume more than TB. By contrast, M2 and M1 octahedra of S95 compress almost identically and the same is observed for TA and TB tetrahedra. If we directly compare the M2 and M1 polyhedral volumes (which mainly determine the bulk compressibility of the orthopyroxene structure, e.g., Thompson et al. 2005; Nestola et al. 2006) in S95 and Ca-opx, we can see that in the same pressure range (up to 6.25 GPa) the M1 volume of Ca-opx compresses slightly more than that of S95 (6.1% against 5.0%). As mentioned earlier, the presence of Fe appears to make M1 more resistant to contraction (as demonstrated by en_{60} orthopyroxene), and it also makes M1 in S95 stiffer than the pure Mg site in the Ca-opx. A very small difference in compressibility between the two latter could be due to the simultaneous presence of Al in M1 of S95, which seems to counterbalance the effect of Fe.

Concerning the M2 polyhedron, differences between Ca-opx and S95 are much more marked. M2 volume decreases by about 7.7% for Ca-opx, whereas for S95 it decreases by only 4.7% (up to 6.25 GPa). This large difference is also related to the tetrahedral chain kinking. The B chain shows the most pronounced kinking (defined by the O3B-OB-O3B angle) in both S95 and Ca-opx. In Figure 7, the evolution of the O3B-O3B-O3B angle for Ca-opx and S95 is reported as a function of pressure. It can be seen that for Ca-opx the kink (which is inverse to the angle) increases strongly at constant rate. In S95 the B chains are more kinked at room pressure, but the increase of kink (and the chain contraction) is slower than in the Ca-opx, and the two structures achieve the same value at about 4 GPa. At higher pressures the chain kink (contraction) in S95 continues at an even smaller rate. The consequence of this is that total contraction of the B chain in S95 is about 1.2% at 6.25 GPa, whereas the chain in Ca-opx contracts by 3.5%. It can be supposed that the kink of the B tetrahedral chain is dependent on the mismatch between the size of the TB tetrahedron and the size of the M2 octahedron. As shown on Figure 8, the longest bond to M2 is formed by the O3B oxygen, which is at the same time the bridging oxygen of the B tetrahedral chain. As mentioned earlier, this bond also shows the largest contraction during the compression of the orthopyroxene structure. That the kink of the B tetrahedral chain reflects the relation between the sizes of the M2 and TB coordination polyhedra, is confirmed by Figure 9, which shows the ratio of the two volumes as a function of pressure for S95, Ca-opx and pure enstatite. One can see that Figures 7 and 9 depict one and the same effect.

The evolution of the volumes of M coordination polyhedra and their distortion parameters as a function of pressure shows a non-linear dependence. As noted by Hugh-Jones et al. (1997) the compressibility of tetrahedra increases with increasing pressure. Our plot on Figure 5 would not confirm this general trend. Figure 3 shows that the compressibility of the octahedral coordinations generally decreases with increasing pressure.

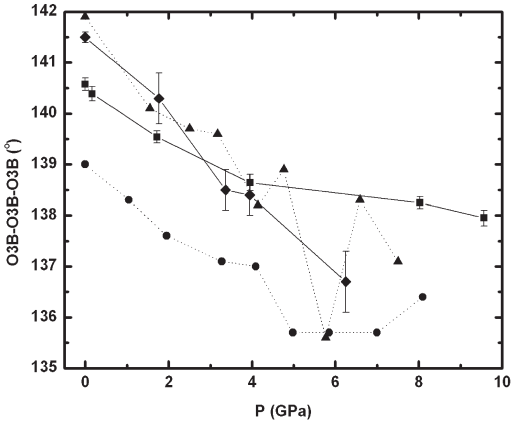

FIGURE 7. Evolution with pressure of the O3B-O3B-O3B angle (°) describing the tetrahedral B chain kinking for the sample S95 (squares) studied in this work and the Ca-bearing orthopyroxene (rhombs) (Nestola et al. 2006). Also added are the data for synthetic enstatite (Hugh-Jones and Angel 1994) (circles) and synthetic en_{60} orthopyroxene (Hugh-Jones et al. 1997) (triangles). The atomic coordinates of atoms for the two latter structures are taken from AMS crystal structure database and therefore the standard deviations are not available; however we could expect that they are slightly higher than S95 and Ca-bearing orthopyroxene.

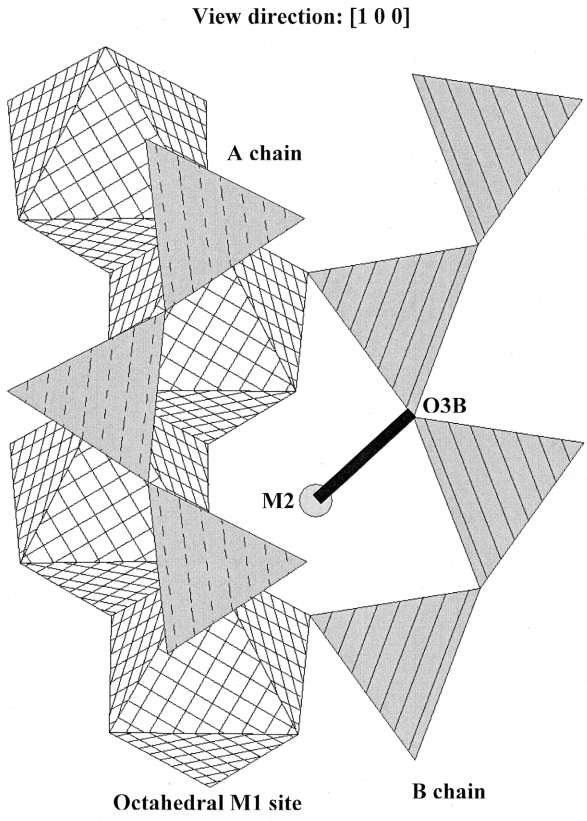

FIGURE 8. Part of the crystal-structure of S95 sample studied in this work viewed along the [100] direction. The tetrahedral B chain is depicted in gray and solid lines and the tetrahedral A chain in gray and dashed lines. The octahedral M1 sites are in white and crossed lines. The black thick line corresponds to the M2-O3B bond.

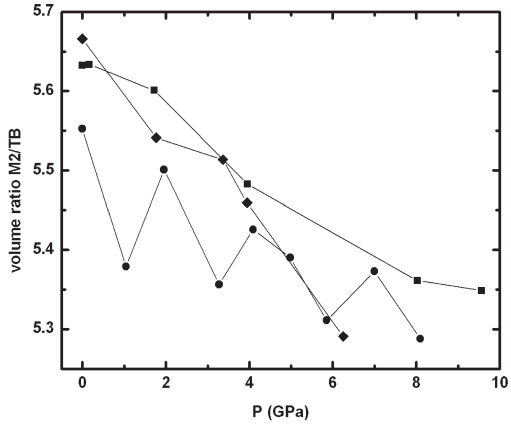

FIGURE 9. Evolution of the ratio between the volumes of M2 and TB in S95 (squares) studied in this work, the Ca-bearing orthopyroxene (Nestola et al. 2006) (rhombs) and the synthetic enstatite (Hugh-Jones and Angel 1994) (circles). To be compared with Figure 7.

An exception is Ca-opx in which the compressibility of M2 polyhedron increases with pressure. The changes in the trends of compression of various polyhedra evidently result in a relatively large value of K' characteristic for orthopyroxenes. The observed large variations in K', and their dependence of atomic substitutions in the structure, can be related to the effects these substitutions have on the relative compressibilities of different coordination polyhedra.

Finally, a comparison of the linear axial compressibility between S95 and Ca-opx shows that β_a and β_b are quite similar, whereas β_c is significantly higher (by more than 10%) for Ca-opx, in agreement with the observation that the B chain running along the **c** direction of Ca-opx is much more compressible than that of the S95 sample.

ACKNOWLEDGMENTS

We thank Fritz Seifert for providing the S95 sample and for helpful scientific discussions on orthopyroxenes and Rolf Berg from the Technical University of Denmark. We also thank Robert Downs and Geoffrey Bromiley for their review and M. Kunz for several suggestions that strongly improved the manuscript.

REFERENCES CITED

Angel, R.J. (2001) Equation of state. In R.M. Hazen and R.T. Downs, Eds., High-temperature and High-pressure Crystal Chemistry, 41, p. 35–59. Reviews in Mineralogy and Geochemistry, Mineralogical Society of America, Chantilly, Virginia.

——— (2002) EOS-FIT5.2. Computer program. Crystallography Laboratory, Department of Geological Sciences, Virginia Tech, Blacksburg, U.S.A.

Angel, R.J. and Hugh-Jones, D.A. (1994) Equation of state and thermodynamic properties of enstatite pyroxenes. Journal of Geophysical Research, 99, 19777–19783.

Angel, R.J. and Jackson, J.M. (2002) Elasticity and equation of state of orthoenstatite, $MgSiO_3$. American Mineralogist, 87, 558–561.

Angel, R.J., Allan, D.R., Miletich, R., and Finger, L.W. (1997) The use of quartz as an internal pressure standard in high-pressure crystallography. Journal of Applied Crystallography, 30, 461–466.

Angel, R.J., Downs, R.T., and Finger, L.W. (2000) High-temperature-high-pressure diffractometry. In R.M. Hazen and R.T. Downs, Eds., High-temperature and High-pressure Crystal Chemistry, 41, p. 559–596. Reviews in Mineralogy and Geochemistry, Mineralogical Society of America, Chantilly, Virginia.

Balić-Žunić, T. (2007) Use of three-dimensional parameters in the analysis of crystal structures under compression. In A. Grzechnik, Ed., Pressure Induced Phase Transitions. Transworld Research Network, Kerala, India.

Balić-Žunić, T. and Makovicky, E. (1996) Determination of the Centroid or "the Best Centre" of a Coordination Polyhedron. Acta Crystallographica, B52, 78–81.

Balić-Žunić, T. and Vicković, I. (1996) IVTON—Program for the calculation of geometrical aspects of crystal structures and some crystal chemical applications. Journal of Applied Crystallography, 29, 305–306.

Birch, F. (1947) Finite elastic strain of cubic crystals. Physical Review, 71, 809–824.

Boffa Ballaran, T., Balić-Žunić, T., Nestola, F., and Stalder, R. (2006) The effect of Al and water substitution on the high-pressure behavior of orthoenstatite. Eleventh International Conference on Experimental Mineralogy, Petrology and Geochemistry, Volume of the Abstracts, p. 10.

Bromiley, G.D. and Bromiley, F.A. (2006) High-pressure phase transitions and hydrogen incorporation into $MgSiO_3$ enstatite. American Mineralogist, 91, 1094–1101.

Cámara, F. and Nestola, F. (2006) Anomalous thermal expansion in Ca-rich orthoenstatite. Eleventh International Conference on Experimental Mineralogy, Petrology and Geochemistry, Volume of the Abstracts, p. 13.

Gatta, G.D., Rinaldi, R., Knight, K.S., Molin, G., and Artioli, G. (2007) High-temperature structural and thermoelastic behavior of mantle orthopyroxenes: An in situ neutron powder diffraction study. Physics and Chemistry of Minerals, 34, 185–200.

Hugh-Jones, D.A. and Angel, R.J. (1994) A compressional study of $MgSiO_3$ orthoenstatite up to 8.5 GPa. American Mineralogist, 79, 405–410.

Hugh-Jones, D.A., Chopelas, A., and Angel, R.J. (1997) Tetrahedral compression in $(Mg,Fe)SiO_3$ orthopyroxenes. Physics and Chemistry of Minerals, 24, 301–310.

King, H.E. and Finger, L.W. (1979) Diffracted beam crystal centering and its application to high-pressure crystallography. Journal of Applied Crystallography, 12, 374–378.

Miyake, A., Shimobayashi, N., and Kitamura, M. (2004) Isosymmetric structural phase transition of orthoenstatite: Molecular dynamics simulation. American Mineralogist, 89, 1667–1672.

Nestola, F., Gatta, G.D., and Boffa Ballaran, T. (2006) The effect of Ca substitution on the elastic and structural behavior of orthoenstatite. American Mineralogist, 91, 809–815.

Perrillat, J.P., Nestola, F., Sinogeikin, S.V., and Bass, J.D. (2007) Single-crystal elastic properties of $Ca_{0.07}Mg_{1.93}Si_2O_6$ orthopyroxene. American Mineralogist, 79, 405–410.

Ralph, R.L. and Finger, L.W. (1982) A computer program for refinement of crystal orientation matrix and lattice constants from diffractometer data with lattice symmetry constraints. Journal of Applied Crystallography, 15, 537–539.

Robinson, K., Gibbs, G.V., and Ribbe, P.H. (1971) Quadratic elongation; a quantitative measure of distortion in coordination polyhedra. Science, 172, 567–570.

Sheldrick, G.M. (1997) Programs for crystal structure analysis (Release 97-2). Institüt für Anorganische Chemie der Universität, Tammanstrasse 4, D-3400 Göttingen, Germany.

Tazzoli, V. and Domeneghetti, M.C. (1987) Crystal-chemistry of natural and heated aluminous orthopyroxenes. Physics and Chemistry of Minerals, 15, 131–139.

Thompson, R.M., Downs, R.T., and Redhammer, G.J. (2005) Model pyroxenes III: Volume of $C2/c$ pyroxenes at mantle P, T, and x. American Mineralogist, 90, 1840–1851.

MANUSCRIPT RECEIVED MAY 14, 2007
MANUSCRIPT ACCEPTED NOVEMBER 21, 2007
MANUSCRIPT HANDLED BY MARTIN KUNZ